IOP Publishing Nanotechnology
Nanotechnology **26** (2015) 115201 (8pp) doi:10.1088/0957-4484/26/11/115201

Strain-induced conduction gap in vertical devices made of misoriented graphene layers

V Hung Nguyen[1,2], Huy-Viet Nguyen[2], J Saint-Martin[1] and P Dollfus[1]

[1] Institut d'Electronique Fondamentale, UMR8622, CNRS, Université Paris Sud, 91405 Orsay, France
[2] Center for Computational Physics, Institute of Physics, Vietnam Academy of Science and Technology, PO Box 429 Bo Ho, 10000 Hanoi, Vietnam

E-mail: hung@iop.vast.ac.vn

Received 19 November 2014, revised 19 January 2015
Accepted for publication 26 January 2015
Published 24 February 2015

Abstract

We investigate the effects of uniaxial strain on the transport properties of vertical devices made of two misoriented (or twisted) graphene layers, which partially overlap each other. We find that because of the different orientations of the two graphene lattices, their Dirac points can be displaced and separated in the *k*-space by the effects of strain. Hence, a finite conduction gap as large as a few hundred meV can be obtained in the device with a small strain of only a few percent. The dependence of this conduction gap on the strain magnitude, strain direction, channel orientation and twist angle are clarified and presented. On this basis, the strong modulation of conductance and significant improvement of Seebeck coefficient are shown. The suggested devices therefore may be very promising for improving applications of graphene, e.g., as transistors or strain and thermal sensors.

Keywords: graphene, strain engineering, energy-gap

(Some figures may appear in colour only in the online journal)

The continuing interest in graphene, a two-dimensional (2D) monolayer arrangement of carbon atoms, as conducting material is one of the most striking trends of research in solid-state and applied physics over the last decade [1–7]. It is due in particular to the specific band structure of this material, i.e., with gapless conical shape at six corners of the hexagonal Brillouin zone and the Dirac character of low-energy excitations, which leads to many peculiar effects such as, for instance, relativistic-like behavior of charge carriers, finite value of the conductivity at zero density, unusual quantum Hall effect, etc [1]. It is due also to outstanding properties such as high carrier mobility, small spin–orbit coupling, high thermal conductivity and excellent mechanical properties, which make it very promising for a broad range of applications. However, in the operation of electronic devices, graphene still has serious drawbacks associated with the lack of an energy bandgap in its electronic structure. In particular, graphene transistors have a low ON/OFF ratio and poor current saturation [8]. Many efforts of bandgap engineering in graphene have been made to solve these issues. For instance, techniques such as cutting 2D graphene sheet into narrow nanoribbons [9], depositing graphene on hexagonal boron nitride (hBN) substrate [10], nitrogen-doped graphene [11], applying an electric field perpendicularly to Bernal-stacking bilayer graphene [12], graphene nanomeshes [13], using hybrid graphene/hBN [14] or vertical graphene channels [15] have been explored. Although they are certainly promising options for opening a bandgap in graphene, each of them still has its own issues. Hence, bandgap engineering is still a timely and desirable topic at the moment for the development of graphene in nanoelectronics.

Besides the points mentioned above, graphene is an attractive material for flexible electronics since it is able to sustain a much larger (i.e., >20% [5]) strain than other semiconductors. Recently, some techniques [16, 17] to generate extreme strain in graphene in a controllable and non-destructive way have also been explored. Interestingly, strain engineering has been suggested as an approach to efficiently

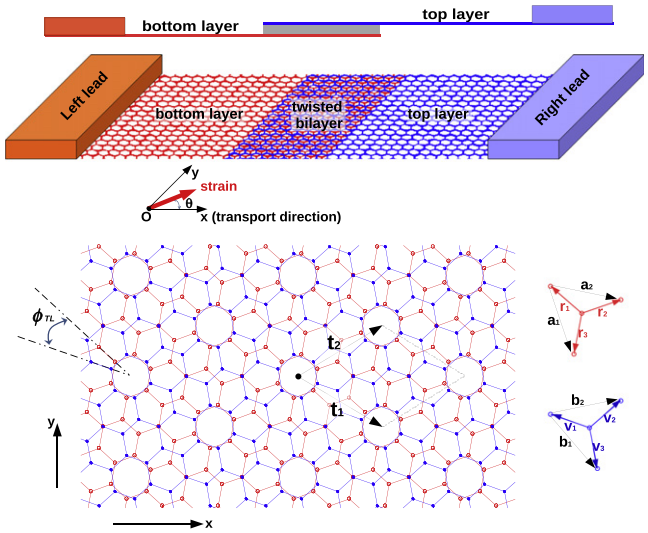

Figure 1. Schematic of vertical graphene devices investigated in this work (middle) and their side view (top). The bottom shows the top view of a typical misoriented (usually called 'twisted') graphene bilayer lattice with the primitive vectors $\vec{t}_{1,2}$. The bottom right presents the zoom images showing the nearest-neighbor vectors $\vec{n}_{1,2,3}$ ($\vec{v}_{1,2,3}$) and lattice vectors $\vec{a}_{1,2}$ ($\vec{b}_{1,2}$) of the bottom (top) layer.

modulate the electronic structure of graphene nanomaterials. On this basis, many interesting electrical, optical and magnetic properties induced by strain have been investigated, e.g., see [18–32]. Remarkably, although the slightly strained (i.e., a few percent) 2D graphene remains semimetallic [19], strain has been demonstrated as a technique for strongly improving the applications of some particular graphene channels, for instance, graphene nanoribbons with a local strain [22, 25], graphene with grain boundaries [24] and graphene strain junctions [26, 27].

Recently, the interest of the graphene community has also been oriented toward the investigation of twisted graphene few-layer lattices. They are actually few-layer graphene lattices where one layer is rotated relative to another layer by an arbitrary angle and can form a Moiré pattern. These graphene lattices often appear in the thermal decomposition of the C-face of SiC or in the copper-assisted growth using chemical vapor deposition method, e.g., see [33–38]. In the twisted graphene bilayer, the bandstructure changes dramatically [39–41], compared to that of monolayer or Bernal/AA stacking bilayer systems. In addition to the existence of linear dispersion in the vicinity of K-points, saddle points emerge at the crossing of Dirac cones, yielding van Hove singularities in the density of states at low energies, and the Fermi velocity to be remarkably renormalized. Moreover, the phonon transport in these systems exhibits a strong dependence on the twist angle [42]. Motivated by recent studies [24, 26, 27] of the strain effects to generate/modulate the conduction gap in graphene channels, we investigate in this work the effects of uniaxial strain on the charge transport in vertical devices made of two misoriented graphene layers as schematized in figure 1. The idea is as follows: in any hetero-channels made of different graphene sections where their Dirac cones are located at different positions in the k-space, the transmission probability (and hence conductance/current) shows finite energy gaps, i.e., conduction gaps, even though these graphene sections are still metallic (similarly, see the detailed explanation in [24, 27]). This feature is also expected to be observed here because the graphene lattices in the left and right sides have different orientations and hence their electronic structures should be, in principle, different when a strain is applied. Moreover, compared to the vertical devices [15] and strain hetero-channels [26, 27] previously studied, the advantages of these devices come from the use of a uniform strain and graphene materials only, which can make it a simple option for the fabrication process.

For the investigation of charge transport in the proposed devices, we employed atomistic tight-binding calculations as in [19, 26, 27, 40, 43]. Here, we assume that: (i) two (bottom and top) graphene sheets partially overlap each other and the transport (i.e., Ox) direction is perpendicular to this overlap section as shown in figure 1; (ii) the top sheet is rotated relative to the bottom one by a commensurate angle $\phi_{\rm TL}$; (iii) a uniformly uniaxial strain is applied in the in-plane direction with an arbitrary angle θ with respect to the transport direction. The commensurate angles are determined by $\cos\phi_{\rm TL} = (n^2/2 + 3mn + 3m^2)/(n^2 + 3mn + 3m^2)$ [43], where n and m are coprime positive integers. The primitive vectors shown in figure 1 are determined as follows: $\vec{t}_1 = m\vec{a}_1 + (n+m)\vec{a}_2$ and $\vec{t}_2 = -(n+m)\vec{a}_1 + (n+2m)\vec{a}_2$ if $\gcd(n, 3) = 1$; $\vec{t}_1 = \left(\frac{n}{3} + m\right)\vec{a}_1 + \frac{n}{3}\vec{a}_2$ and $\vec{t}_2 = -\frac{n}{3}\vec{a}_1 + \left(\frac{2n}{3} + m\right)\vec{a}_2$ if $\gcd(n, 3) = 3$ (where $\gcd(p, q)$ is the greatest common divisor of p and q). The detailed description of the two lattice types corresponding to $\gcd(n, 3) = 1$ and 3 can be found in [43]. For simplicity, throughout the work, unless otherwise stated the channel orientation as schematized in figure 1 is considered, i.e., the transport direction is parallel to the vector $\vec{L}_0 = \vec{t}_1 + \vec{t}_2$. The strain causes changes in the $C{-}C$ bond vector $\vec{r}_{ij}$ according to $\vec{r}_{ij}(\sigma) = \{\mathbb{1} + M_s(\sigma, \theta)\}\vec{r}_{ij}(0)$ with the strain tensor

$$M_s(\sigma, \theta) = \sigma \begin{bmatrix} \cos^2\theta - \gamma\sin^2\theta & (1+\gamma)\sin\theta\cos\theta \\ (1+\gamma)\sin\theta\cos\theta & \sin^2\theta - \gamma\cos^2\theta \end{bmatrix}$$

where σ represents the strain and $\gamma \simeq 0.165$ is the Poisson ratio [45]. Taking into account the strain effects, the hopping parameters are adjusted accordingly as in [19], i.e., $t_{ij}(\sigma) = t_{ij}(0)\exp\left[-3.37\left\{r_{ij}(\sigma)/r_{ij}(0) - 1\right\}\right]$. To compute the transport quantities (transmission probability and conductance) and extract the value of conduction gap, we used the non-equilibrium Green's function technique and the bandstructure analysis described in [26, 27]. In particular, the conductance is computed from the standard Landauer formula:

$$G(E_{\rm F}) = \frac{e^2 W}{\pi h}\int_{BZ} {\rm d}k_y \int_{-\infty}^{\infty} {\rm d}\epsilon \mathcal{T}(\epsilon, k_y)\left[-\frac{\partial f_{\rm F}(\epsilon)}{\partial\epsilon}\right] \quad (1)$$

where W is the channel width (i.e., its size along the Oy axis), the transmission probability $\mathcal{T}(\epsilon, k_y)$ is determined from the

Green's functions [46], and $f_F(\epsilon) = \left[1 + \exp\left(\frac{\epsilon - E_F}{k_B T}\right)\right]^{-1}$ is the Fermi distribution function with the Fermi energy E_F at the contacts. Here, we consider the case where the lateral size (along the Oy direction) of graphene channel is much larger than the length (along the Ox direction) of the active region between the two contacts (see figure 1). Within this assumption, the influence of channel edges and lateral confinement effects are neglected. They are important only for narrow graphene nanoribbons. On this basis, the extension along the Oy direction can be considered through Bloch boundary conditions [26, 27]. The integration over k_y in equation (1) is performed in the first Brillouin zone.

The conduction gap mentioned here is essentially the energy window within which the Fermi energy can be varied (e.g., by applying and tuning a back gate voltage) while the channel remains insulating. Therefore, this gap can be determined either as the gap of conductance in equation (1) at zero temperature or by analyzing the bandstructures of left and right graphene sections, i.e., bottom and top graphene layers, respectively. The details of these calculations have been reported in [27]. Since the conductance is computed from equation (1), the appearance of a conduction gap is essentially governed by the gaps of transmission probability, which is fully related to the energy gaps in the semi-infinite graphene sections in the left and right sides. These energy gaps can be defined directly from the graphene bandstructures. Hence, the conduction gap can be determined using the following two steps. From the bandstructures $E_{bot}(\vec{k})$ and $E_{top}(\vec{k})$ obtained by solving the tight-binding Hamiltonian, we first calculate the energy gaps $E_{bot}^{gap}(k_y)$ and $E_{top}^{gap}(k_y)$ as a function of k_y for the bottom and top graphene layers, respectively. The maximum of these energy gaps determines the gap $E_{dev}^{gap}(k_y)$ of transmission probability through the device channel. The conduction gap E_{gap} is then obtained as the minimum value of $E_{dev}^{gap}(k_y)$ when varying k_y in the whole Brillouin zone. The equivalence of these two methods has been actually demonstrated, as for instance in the detailed discussions on figures 3 and 4 in [27].

Note that because of the lattice symmetry, the channels with twist angles $\phi_{TL} = 30° - \alpha$ and $30° + \alpha$ (similarly, for ϕ_{TL} and $-\phi_{TL}$) have the same transport properties. This limits our investigation to $\phi_{TL} \in [0, 30°]$ and ϕ_{TL} is hence identical to the smallest angle between the armchair (or zigzag) directions of two graphene layers (see in figure 1), which can fully characterize the misalignment. Moreover, the applied strain of angle θ is identical to that of $\theta + 180°$ and hence we only consider the strain angles $\theta \in [-90°, 90°]$. Actually, the possibilities of controlling the direction of strain applied to the graphene channel have been demonstrated in several experiments, e.g., in [47, 48]. In particular, the authors of [48] fabricated a system where graphene is transferred to a polydimethylsiloxane substrate and have shown that it is possible to control the strain direction by changing the stretching direction of the substrate. This could be a good approach to realize our proposed device.

In figure 2, we present $E - k_y$ maps showing the main effects of strain on the transmission probability of considered devices in two cases of $\phi_{TL} \simeq 21.8°$ (i.e., $n = m = 1$) and $\phi_{TL} \simeq 27.8°$ (i.e., $n = 3$, $m = 2$). First, the device remains metallic with a zero conduction gap in the case of unstrained layers (see figures 2((a), (e))). This is because the Dirac cones of graphene sections in the left and right sides are located at the same k_y-position, i.e., at the K-point. The strain can induce a displacement of Dirac cones from the K-point [19, 27] and a finite gap can open in the device if the Dirac cones of two such graphene sections are separated along the k_y-direction, similarly to what was explained in [27]. Therefore, the transport picture is dramatically changed as shown in figures 2((b)–(d), (f)). In figure 2(b), although the Dirac cones are displaced, the device is still metallic with a zero conduction gap. This is essentially explained by the fact that the system is symmetric with respect to the overlap region (i.e., the Oy direction) even when the strain of 3% with $\theta = 0°$ is applied. Because of this symmetry, the Dirac cones of the left and right sections are still located at the same k-point, which explains the zero gap observed. This symmetry can be broken when the direction of applied strain changes, leading to the opening of a finite conduction gap as seen in figures 2((c), (d), (f)). In the case of $\phi_{TL} \simeq 21.8°$, finite gaps of ~ 240 meV and 390 meV are achieved for the strain angles $\theta = 20°$ and 45°, respectively. When changing the twist angle ϕ_{TL}, we observed similar properties; however, the value of conduction gap for a given strain is dependent on ϕ_{TL}. In particular, the gap of ~ 305 meV is obsered for the strain $\{3\%, 45°\}$ in the case of $\phi_{TL} \simeq 27.8°$ in figure 2(f). Thus, these data show the following important features: (i) the strain can induce a finite conduction gap in the device under study; and (ii) besides the strain magnitude, the gap is strongly dependent on the strain direction and twist angle. Similar features have been also reported in [27] for monolayer graphene strain junctions.

In figure 3, we display pictures showing the properties of conduction gap in the device discussed above with respect to the strain magnitude, strain direction and channel orientation while the twist angle $\phi_{TL} \simeq 21.8°$ is fixed. We first discuss the results in figure 3(a) obtained in the L_0-case where the transport direction is parallel to $\vec{L}_0 = \vec{t}_1 + \vec{t}_2$ and the strain magnitude $\sigma = 3\%$ is applied. It is shown that the conduction gap is a function of strain direction θ with two peaks at $\theta \simeq \pm 45°$ and zero values for $\theta = 0°$ and $\pm 90°$. The reason why the gap is zero at $\theta = \pm 90°$ is essentially similar to that for which the zero gap is observed at $\theta = 0°$ explained above. Figures 3((b), (c)) present the maps of conduction gap with respect to the strain magnitude and its applied direction in the tensile and compressive cases, respectively. In addition, it is shown that (i) the gap almost linearly increases with the strain magnitude; (ii) for a given magnitude, the compressive strain gives a larger gap than the tensile one; (iii) differently from the strain junctions in [27], both kinds of strain give a similar dependence of conduction gap on the strain direction. Finally, since it is due to the separation of Dirac cones in the k_y-axis, the conduction gap will also be dependent on the channel orientation. In figure 3(a), we additionally display the data

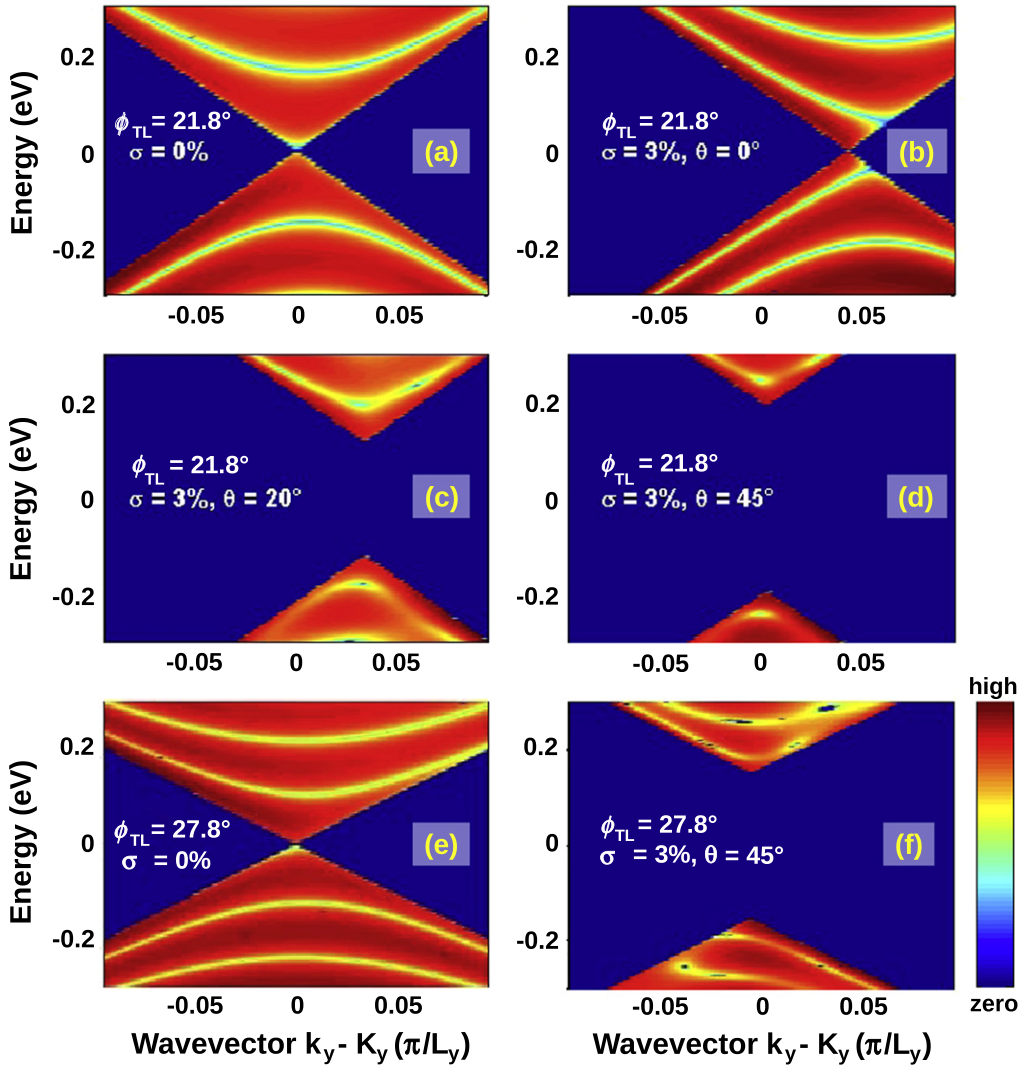

Figure 2. $(E - k_y)$ maps of transmission probability of considered devices around the Dirac point with different applied strains and twist angles. $L_y \equiv \|\vec{t}_2 - \vec{t}_1\|$ is the size of unit cells in the Oy-direction.

obtained for two other channel orientations L_1 and L_2 (see the top-right images), compared to that of L_0. Note that in the two cases of $L_{1,2}$, the transport direction is parallel to the armchair direction of the top and bottom layers, respectively, while as mentioned above, it is parallel to the vector $\vec{L}_0 = \vec{t}_1 + \vec{t}_2$ in the L_0-case. Indeed, our calculations show that in general, a finite conduction gap can always be observed but its dependence on the strain direction is dramatically changed when changing the channel orientation. In particular, as seen in figure 3(a), the $E_{\text{gap}}(\theta)$ function exhibits two similar peaks and two valleys in all cases but the position of these peaks/valleys strongly depends on the channel orientation.

Next, we explore the properties of conduction gap with respect to the twist angle ϕ_{TL}. In figure 4, we display the data obtained for two types of commensurate lattices [43] corresponding to gcd$(n, 3) = 1$ (lattice 01) and gcd$(n, 3) = 3$ (lattice 02). In addition, we consider separately the two regimes of large ϕ_{TL} (>7.3°) in figure 4(a) and small ϕ_{TL} in figure 4(c). In the regime of large ϕ_{TL}, we find that the similar $E_{\text{gap}}(\theta)$ behavior with finite peaks is observed for all cases investigated: $E_{\text{gap}}-$ peaks are at $\theta \simeq \pm 45°$ and zero values at $\theta = 0°$ or $\pm 90°$. More interestingly, two types of twisted lattices show opposite trends of conduction gap when increasing the twist angle, ϕ_{TL}: E_{gap}-peaks increase for the lattice type 02, while they are generally reduced in the case of the type 01. This phenomenon can be explained by the difference in the symmetry of these two lattice types. By way of illustration, we present a diagram in figure 4(b) showing the displacement and separation of Dirac cones of two graphene layers under strain of angle $\theta = 45°$. The diagram shows that although their displacement is similar for all cases, the separation of Dirac cones of two graphene layers have different behaviors, especially along the k_y direction. For the lattice type 02, this separation tends to increase when increasing the twist angle, while it reduces for the lattice type 01. These properties basically explain the results obtained.

In the regime of small ϕ_{TL}, we find as shown in figure 4(c) another trend of $E_{\text{gap}}(\theta)$ in the case of lattices 01,

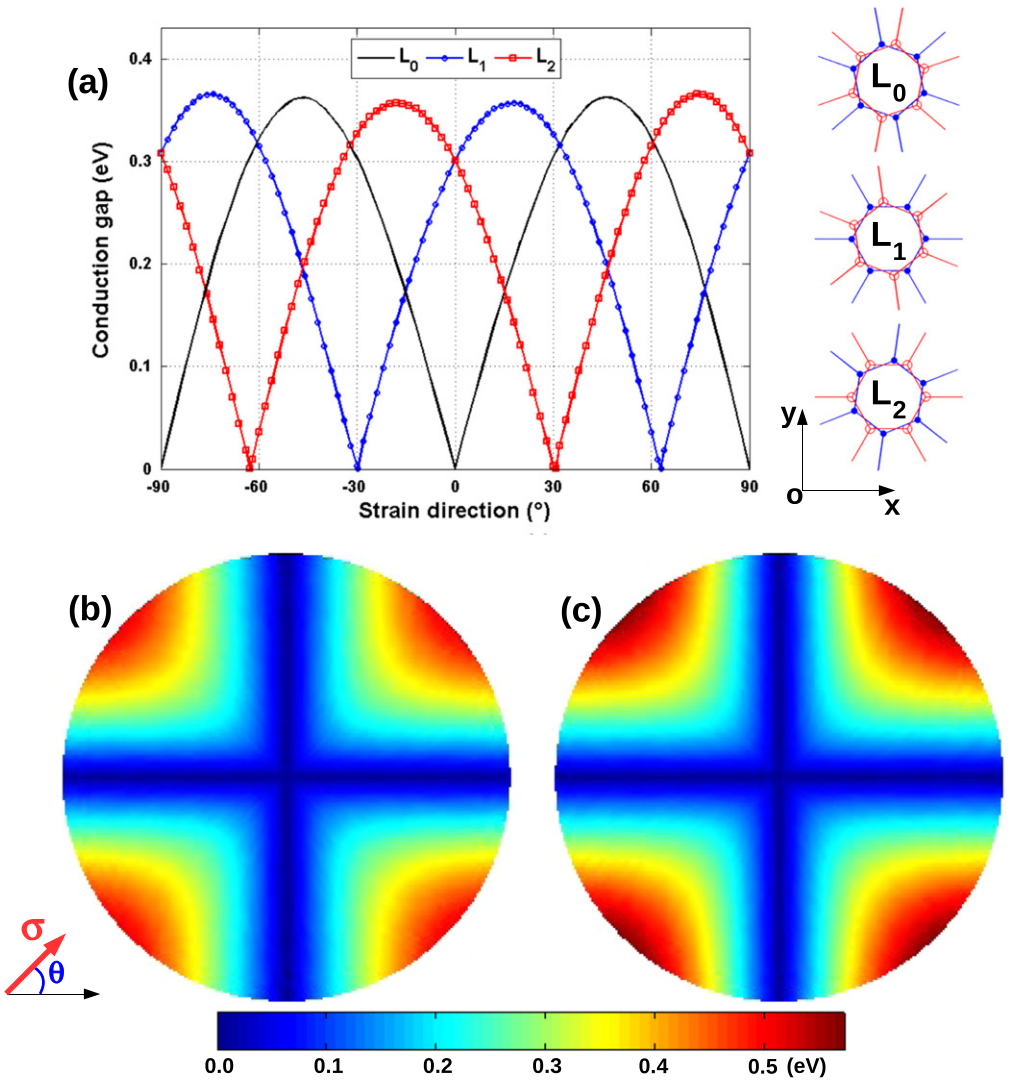

Figure 3. (a) Conduction gap as a function of strain direction ($\sigma = 3\%$) with different channel orientations $L_{0,1,2}$ (see the top-right images). The twist angle $\phi_{TL} \simeq 21.8°$ is considered here. The bottom shows the maps of conduction gap in the L_0-case with respect to the ((b) tensile and (c) compressive) strain and its applied direction. In these maps, the radius from the central point represents the strain magnitude ranging from 0 (center) to 4% (edge).

i.e., E_{gap} quite surprisingly reduces around $\theta = \pm 45°$ when decreasing ϕ_{TL}, in contrast with the results obtained for large ϕ_{TL} in figure 4(a). This feature can be explained as follows (see also the diagrams in figure 4(d)). First, let us remember that (i) each graphene layer has two Dirac cones in the first Brillouin zone and (ii) the value of conduction gap is basically proportional to the smallest distance Δk_y^D between Dirac cones of two layers in the k_y-axis, i.e., between the red and blue symbols in the first Brillouin zone schematized in the top diagram of figure 4(d) (similarly, see the detailed discussion in [27]). At $\theta = -90°$ (similarly, at $\theta = 0°$ or 90°), $\Delta k_y^D = 0$ and the gap is hence zero. When θ increases from $-90°$, Δk_y^D and, thus, E_{gap} increase. The peak of E_{gap} around $\theta = 45°$ and its reduction when tuning θ from 45° to 0° are simply a consequence of the fact that the movement of Dirac cones changes its direction and the behavior of Δk_y^D is reversed (i.e., from increasing to decreasing) around $\theta = 45°$. These properties are observed in the cases of large ϕ_{TL} displayed in figure 4(a) but another peculiar feature appears in the cases of small ϕ_{TL}: when the strain-induced displacement of Dirac cones is large enough, situations (1) and (2) (see the middle and bottom diagrams of figure 4(d)) can occur. In situation (1), the Dirac cone of the first Brillouin zone can reach its edge and then enter the second zone. Simultaneously, the Dirac cone of the second zone moves in the opposite direction to the first one. In situation (2), the two Dirac cones in the first Brillouin zone move in the opposite directions to the point of $k_y = 0$ and then exchange their places. Both situations can change the behavior of Δk_y^D from increasing to decreasing or vice versa. Note that these situations occur only in the cases where the size of the Brillouin zone is small. That is exactly the case of small ϕ_{TL} considered here where the size of primitive cells is large. For instance, when increasing θ from $-90°$ to $-45°$, the behavior of E_{gap} suddenly changes from increasing to decreasing as shown for $\phi_{TL} = 5.08°$, 3.89°,

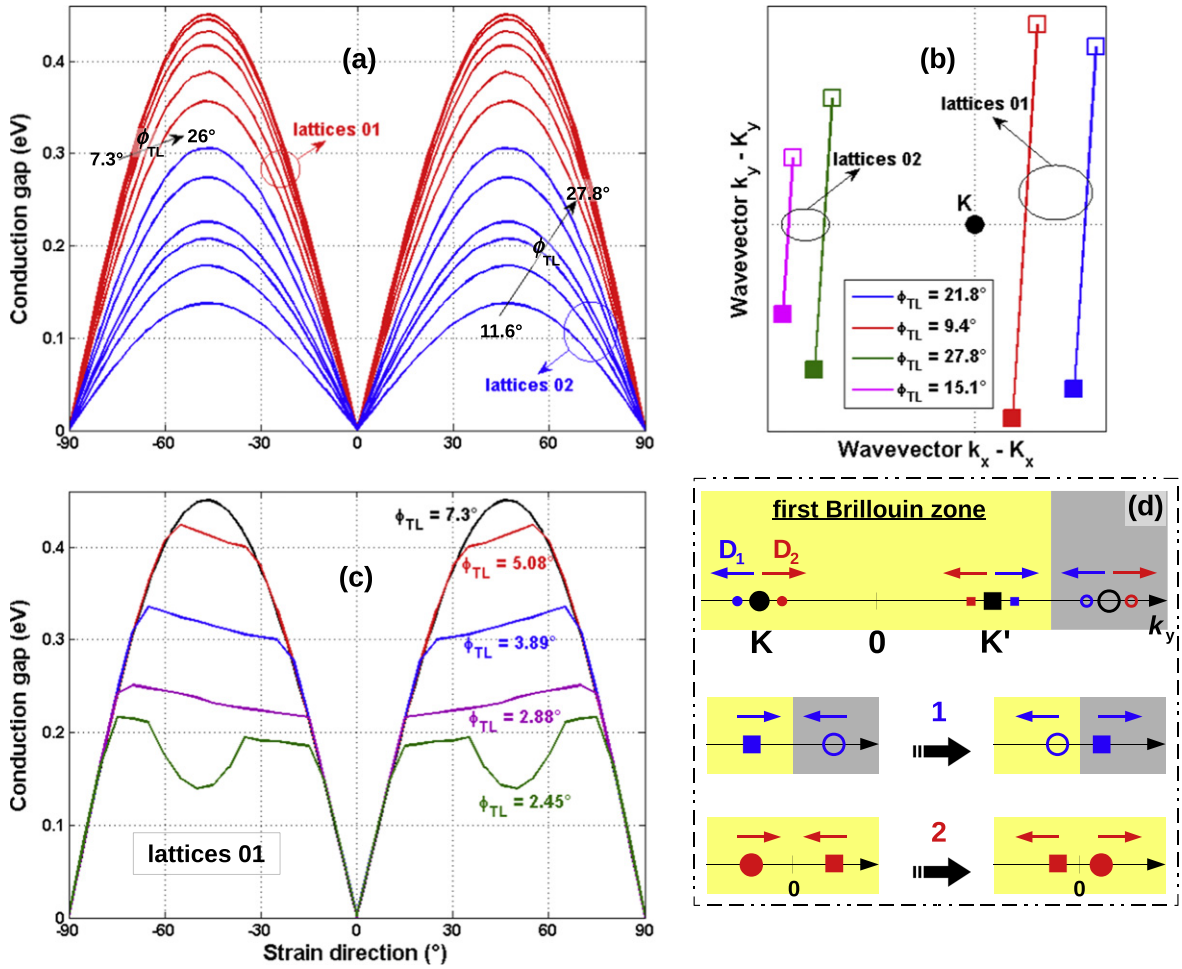

Figure 4. Conduction gap as a function of the strain direction of different twist angles ϕ_{TL}: large ϕ_{TL} (a) and small ϕ_{TL} (c). (b) Diagram illustrating the strain-induced displacement of Dirac cones away from the K-point in the case of $\theta = 45°$. Open (filled) squares denote the Dirac cones of the bottom (top) graphene layers. Two lattice types 01 and 02 (see text) are considered and, everywhere, the strain $\sigma = 3\%$ is applied. (d) Diagram showing the pictures of the movement of Dirac cones along the k_y-axis when changing the strain (see text). The red and blue colors distinguish the Dirac cones of two different layers. Filled and empty symbols show the position of Dirac cones in the first and second Brillouin zones, respectively.

2.88° and 2.45° in figure 4(c). This is essentially because situation (1) occurs. In the case of 2.45°, the valleys of E_{gap} around $\theta = \pm 45°$ are observed because the situation (2) also occurs. Note that, in the case of lattices 02, because both the maximum displacement of Dirac cones along the k_y-axis and the size of the Brillouin zone tend to reduce when decreasing ϕ_{TL}, the features discussed above are not observed. The evolution of maximum values of E_{gap} when changing ϕ_{TL} is summarized in figure 5. When decreasing ϕ_{TL}, the maximum value of E_{gap} decreases monotonically for lattices 02 while it has a peak but also tends to zero for lattices 01. On this basis, it is suggested that to safely achieve a finite conduction gap without requiring good control of the twist angle, designing devices with ϕ_{TL} around/close to 30° should be a good option.

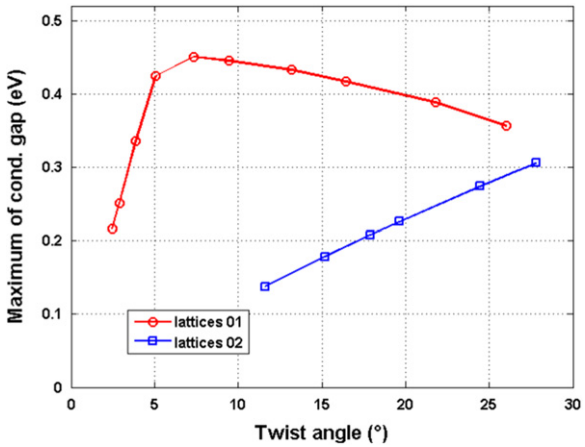

Figure 5. Evolution of maximum values of conduction gap presented in figure 4 with respect to the twist angle ϕ_{TL}.

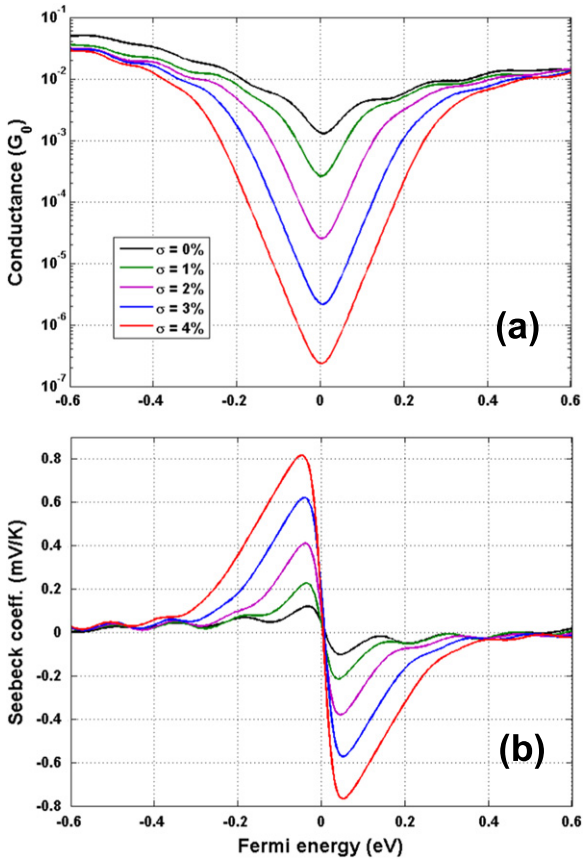

Figure 6. (a) Conductance and (b) Seebeck coefficient with different strain magnitudes at room temperature as a function of Fermi energy. The twist angle is $\phi_{\mathrm{TL}} \simeq 21.8°$ and $\theta = 45°$. $G_0 = e^2W/hL_y$.

Now, we would like to discuss some possible applications of this type of hetero-channel. First, the devices can be used to improve the performance of graphene transistors with the advantage of utilizing a uniform strain and graphene materials only, compared to the vertical devices [15] and strain hetero-channels [26] previously studied. Indeed, as shown in figure 6(a), with a significant conduction gap, these devices can exhibit a very high ON/OFF current ratio, i.e., up to a few ten thousands for a small strain of only ∼3−4%. Second, based on the strong sensitivity of conduction gap to a small strain and its applied direction, this type of device could be an elementary component of strain sensors. Third, the opening of a finite conduction gap also provides a possibility to enhance the thermoelectric properties of these devices by strain. As seen in figure 6(b), the Seebeck coefficient can reach high values of 600 to 800 μV K^{-1} for a strain of ∼3−4% while it is only about a few tens of μV K^{-1} in the unstrained case or in the pristine graphene [49]. This improvement may be significant for applications as thermal sensors [50]. Additionally, although our calculations show that the power factor is still limited and hence the thermoelectric figure of merit *ZT* is small, the phonon conductance is low in this type of device and one can expect that *ZT* can be further improved when including additional energy-gap engineering techniques, e.g., by creating a nanohole lattice in graphene layers as suggested in [44].

Finally, we would like to make some additional remarks. First, in this kind of device, the overlap region between the two layers can have important effects on the transport properties. As in the study on vertical structures with Bernal stacking [44], the size of this region determines, on the one hand, the coupling strength between layers and, on the other hand, the confinement effects (see figure 2) because the electronic structure in the bilayer region is very different from that of the left and right monolayer graphene sections. However, our calculations show that the change in the size of this overlap region does not dramatically change the ON-current (i.e., beyond the gap) except that it can give rise to peaks and shallow valleys in the conductance as seen in figure 6. Second, we would like to point out that besides the use of a uniform strain, the vertical devices studied here have the additional advantage of being able to achieve the same values of conduction gap as the unstrained/strained graphene junctions in [27], but with smaller strain. For instance, a strain of ∼4% is enough to achieve a conduction gap of ≳500 meV, while a strain of ≳6÷7% is required in the latter channels. This improvement comes from the fact that the Dirac cones are displaced by strain in both the left and right graphene sections, while in strained/unstrained junctions, the displacement of Dirac cones occurs only in the strained graphene section. Similar improvement can be achieved in channels made of differently strained graphene lattices, e.g., compressive/tensile strained junctions [27]. However, the control of this complicated strain profile may be a practical issue. Third, besides the case of uniform strains studied here, similar effects can still be obtained in these devices if the strain is applied to only one layer or two different strains to two layers [51]. In such cases, the properties of E_{gap} should, of course, be strongly dependent on the strain configurations.

In conclusion, we have investigated effects of uniaxial strain on the transport properties of vertical devices made of two misoriented (twisted) graphene layers. It was shown that strain can induce the displacement of Dirac cones of both layers and because of their different orientations, these Dirac cones can be separated in the *k*-space. As a consequence, the device channel can be tuned from metallic to semiconducting by strain. A conduction gap larger than 500 meV can be achieved in the device with a small strain of only ∼4%. The dependence of this conduction gap on the strain magnitude, strain direction, channel orientation and twist angle has been clarified. The twist angle $\phi_{\mathrm{TL}} \simeq 30°$ is a good option for a large conduction gap, which is less sensitive to the different types of twisted layers. On this basis, an ON/OFF current ratio as high as a few thousands and a strong improvement of Seebeck coefficient can be achieved. The study has hence demonstrated that these vertical devices are very promising for enlarging the applications of graphene in transistors, strain sensors and thermoelectric devices.

Acknowledgments

This research in Hanoi is funded by Vietnam's National Foundation for Science and Technology Development

(NAFOSTED) under grant number 103.01-2014.24. This work was partially supported by the French ANR through project NOE (12JS03-006-01).

References

[1] Castro Neto A H, Guinea F, Peres N M R, Novoselov K S and Geim A K 2009 *Rev. Mod. Phys.* **81** 109
[2] Wu Y, Farmer D B, Xia F and Avouris P 2013 *Proc. IEEE* **101** 1620
[3] Yazyev O V 2010 *Rep. Prog. Phys.* **73** 056501
[4] Balandin A A 2011 *Nat. Mater.* **10** 569
[5] Sharma B K and Ahn J-H 2013 *Solid State Electron.* **89** 177
[6] Novoselov K S, Fal'ko V I, Colombo L, Gellert P R, Schwab M G and Kim K 2012 *Nature* **490** 192
[7] Schwierz F 2010 *Nat. Nanotechnol.* **5** 487
[8] Meric I, Han M Y, Young A F, Özyilmaz B, Kim P and Shepard K L 2008 *Nat. Nanotechnol.* **3** 654
[9] Han M Y, Özyilmaz B, Zhang Y and Kim P 2007 *Phys. Rev. Lett.* **98** 206805
[10] Kharche N and Nayak S K 2011 *Nano Lett.* **11** 5274
Tang S *et al* 2013 *Sci. Rep.* **3** 2666
[11] Lherbier A *et al* 2013 *Nano Lett.* **13** 1446–50
Zabet-Khosousi A *et al* 2014 *J. Am. Chem. Soc.* **136** 1391–7
[12] Zhang Y, Tang T-T, Girit C, Hao Z, Martin M C, Zettl A, Crommie M F, Shen Y R and Wang F 2009 *Nature* **459** 820
[13] Bai J, Zhong X, Jiang S, Huang Y and Duan X 2010 *Nat. Nanotechnol.* **5** 190
[14] Fiori G, Betti A, Bruzzone S and Iannaccone G 2012 *ACS Nano* **6** 2642
[15] Britnell L *et al* 2012 *Science* **335** 947–50
Britnell L *et al* 2013 *Nat. Commun.* **4** 1794
Yu W J *et al* 2013 *Nat. Nanotechnol.* **8** 952–8
[16] Garza H H P, Kievit E W, Schneider G F and Staufer U 2014 *Nano Lett.* **14** 4107
[17] Shioya H, Craciun M F, Russo S, Yamamoto M and Tarucha S 2014 *Nano Lett.* **14** 1158
[18] Pereira V M and Neto A H Castro 2009 *Phys. Rev. Lett.* **103** 046801
[19] Pereira V M, Castro Neto A H and Peres N M R 2009 *Phys. Rev.* B **80** 045401
[20] Levy N, Burke S A, Meaker K L, Panlasigui M, Zettl A, Guinea F, Castro Neto A H and Crommie M F 2010 *Science* **329** 544
[21] Cocco G, Cadelano E and Colombo L 2010 *Phys. Rev.* B **81** 241412
[22] Lu Y and Guo J 2010 *Appl. Phys. Lett.* **97** 073105
[23] Klimov N N, Jung S, Zhu S, Li T, Alan Wright C, Solares S D, Newell D B, Zhitenev N B and Stroscio J A 2012 *Science* **336** 1557
[24] Kumar S Bala and Guo Jing 2012 *Nano Lett.* **12** 1362
[25] Bahamon D A and Pereira Vitor M 2013 *Phys. Rev.* B **88** 195416
[26] Hung Nguyen V, Viet Nguyen H and Dollfus P 2014 *Nanotechnology* **25** 165201
[27] Chung Nguyen M, Hung Nguyen V, Viet Nguyen H and Dollfus P 2014 *Semicond. Sci. Technol.* **29** 115024
[28] Pereira V M, Ribeiro R M, Peres N M R and Neto A H Castro 2010 *Europhys. Lett.* **92** 67001
[29] Ni G-X, Yang H-Z, Ji W, Baeck S-J, Toh C-T, Ahn J-H, Pereira V M and Özyilmaz B 2014 *Adv. Mater.* **26** 1081
[30] Guinea F, Katsnelson M I and Geim A K 2010 *Nat. Phys.* **6** 30
[31] Low T and Guinea F 2010 *Nano Lett.* **10** 3551
[32] Zhai F and Yang L 2011 *Appl. Phys. Lett.* **98** 062101
[33] de Heer W A *et al* 2007 *Solid State Commun.* **143** 92
[34] Hass J, Varchon F, Millan-Otoya J E, Sprinkle M, Sharma N, de Heer W A, Berger C, First P N, Magaud L and Conrad E H 2008 *Phys. Rev. Lett.* **100** 125504
[35] Carozo V, Almeida C M, Ferreira E H M, Cancado L G, Achete C A and Jorio A 2011 *Nano Lett.* **11** 4527
[36] Lucian A, Li G, Reina A, Kong J, Nair R R, Novoselov K S, Geim A K and Andrei E Y 2011 *Phys. Rev. Lett.* **106** 126802
[37] Havener R W, Zhuang H, Brown L, Hennig R G and Park J 2012 *Nano Lett.* **12** 3162
[38] Lu C-C, Lin Y-C, Liu Z, Yeh C-H, Suenaga K and Chiu P-W 2013 *ACS Nano* **7** 2587
[39] Lopes dos Santos J M B, Peres N M R and Castro Neto A H 2007 *Phys. Rev. Lett.* **99** 256802
[40] Trambly de Laissardière G, Mayou D and Magaud L 2010 *Nano Lett.* **10** 804
[41] Li G, Luican A, Lopes dos Santos J M B, Castro Neto A H, Reina A, Kong J and Andrei E Y 2010 *Nat. Phys.* **6** 109
[42] Cocemasov A I, Nika D L and Balandin A A 2013 *Phys. Rev.* B **88** 035428
Nika D L, Cocemasov A I and Balandin A A 2014 *Appl. Phys. Lett.* **105** 031904
[43] Lopes dos Santos J M B, Peres N M R and Neto A H Castro 2012 *Phys. Rev.* B **86** 155449
[44] Hung Nguyen V, Chung Nguyen M, Viet Nguyen H, Saint-Martin J and Dollfus P 2014 *Appl. Phys. Lett.* **105** 133105
[45] Blakslee O L, Proctor D G, Seldin E J, Spence G B and Weng T 1970 *J. Appl. Phys.* **41** 3373
[46] Mazzamuto F, Saint-Martin J, Hung Nguyen V, Chassat C and Dollfus P 2012 *J. Comput. Electron* **11** 67
[47] Frank O *et al* 2011 *ACS Nano* **5** 2231
[48] Dong B, Wang P, Liu Z-B, Chen X-D, Jiang W-S, Xin W, Xing F and Tian J-G 2014 *Nanotechnology* **25** 455707
[49] Zuev Y M, Chang W and Kim P 2009 *Phys. Rev. Lett.* **102** 096807
[50] van Herwaarden A W and Sarro P 1986 *Sensors Actuators* **10** 321
[51] Choi S-M, Jhi S-H and Son T-W 2010 *Nano Lett.* **10** 3486